Inorg. Chem. **2008**, *47*, 5259−5266

Inorganic Chemistry
Article

Theoretical Characterization of the Lowest Triplet Excited States of the Tris-(1,4,5,8-tetraazaphenanthrene) Ruthenium Dication Complex

Fabienne Alary,*,† Martial Boggio-Pasqua,† Jean-Louis Heully,† Colin J. Marsden,† and Patricia Vicendo‡

Laboratoire de Chimie et Physique Quantiques, UMR 5626, IRSAMC, CNRS et Université Paul Sabatier, 118 route de Narbonne, 31062 Toulouse, France, and Laboratoire des Interactions Moléculaires et Réactivité Chimique et Photochimique, UMR 5623, CNRS et Université Paul Sabatier, 118 route de Narbonne, 31062 Toulouse, France

Received February 7, 2008

We present a theoretical study of the ground and the lowest triplet excited states of the tris-(1,4,5,8-tetraazaphenanthrene) ruthenium complex $[Ru(tap)_3]^{2+}$. Density functional theory (DFT) was used to obtain the relaxed geometries and emission energies (Δ-SCF), whereas time-dependent DFT (TD-DFT) was used to compute the absorption spectrum. Our calculations have revealed the presence of three low-lying excited-state minima, which may be relevant in the photophysical/photochemical properties of this complex. Two minima with similar energies correspond to the MLCT $^3A_2$ and MLCT ^3B metal-to-ligand charge-transfer states, the first one corresponding to a D_3 structure, whereas the second is a slightly localized C_2 species. The third and lowest one corresponds to the metal-centered MC ^3A state and displays a pronounced C_2 distortion. We have examined for the first time the localized character of the excitation in the computed MLCT states. In particular, we have evaluated the pseudorotation barrier between the Jahn−Teller C_2 MLCT ^3B minima in the moat around the D_3 conical intersection. We have shown that the complex should be viewed as a delocalized $[Ru^{3+}(tap^{-1/3})_3]^{2+}$ complex in the lowest MLCT states, in agreement with subpicosecond interligand electron transfer observed by femtosecond transient absorption anisotropy study. Upper-bound estimates of the MLCT→MC (3 kcal/mol) and MC→MLCT (10 kcal/mol) activation energy barriers obtained from potential energy profiles in vacuum corroborate the high photoinstability of the MLCT states of the $[Ru(tap)_3]^{2+}$complex.

1. Introduction

Molecular architectures based on polypyridyl complexes of d^6 metal ions such as Ru^{II} are currently among the most studied compounds in coordination chemistry. For instance, their unique photoreactivity stems partly from the nature of the triplet excited states and redox properties responsible for specific electron- and energy-transfer processes. Numerous applications can be mentioned in the fields of photochemistry, photophysics, photocatalysis, and biochemistry.[1,2] Recently, Bijeire et al.[3] and Gicquel et al.[4] have shown that ruthenium complexes with high redox potentials such as $[Ru(tap)_3]^{2+}$ and the tris-bipyrazine ruthenium(II) complex $[Ru(bpz)_3]^{2+}$ (Chart 1) may also photosensitize amino acids and proteins via electron-transfer processes, leading to novel photochemical reactions such as the formation of a photoadduct with tryptophan or tyrosine and thus inducing a modification of the redox state of a metallo-enzyme: the superoxide dismutase (SOD-Cu/Zn).

Despite numerous experimental and theoretical works, many open questions persist. For instance, a discussion about the excited electronic structure of one of the most studied complexes, $[Ru(bpy)_3]^{2+}$, is still a topical issue. While it is

* To whom correspondence should be addressed. E-mail: fabienne.alary@irsamc.ups-tlse.fr.
† Laboratoire de Chimie et Physique Quantiques, IRSAMC.
‡ Laboratoire des Interactions Moléculaires et Réactivité Chimique et Photochimique.

(1) Barton, J. K. *Science* **1986**, *233*, 727–734.
(2) Juris, A.; Balzani, V.; Barigelletti, F.; Campagna, S.; Belser, P.; von Zelewsky, A. *Coord. Chem. Rev.* **1988**, *84*, 85–277.
(3) Bijeire, L.; Elias, B.; Souchard, J.-P.; Gicquel, E.; Moucheron, C.; Kirsch-De Mesmaeker, A.; Vicendo, P. *Biochemistry* **2006**, *45*, 6160–6169.
(4) Gicquel, E.; Boisdenghien, A.; Defrancq, E.; Moucheron, C.; Kirsch-De Mesmaeker, A. *Chem. Commun.* **2004**, *23*, 2764–2765.

10.1021/ic800246t CCC: $40.75
Published on Web 05/21/2008

Chart 1. Schematic representation of the 2,2′-bipyridine (bpy) and 3,3′-bipyrazine (bpz) ligands and the tris-1,4,5,8-tetraazaphenanthrene ruthenium complex $[Ru(tap)_3]^{2+}$

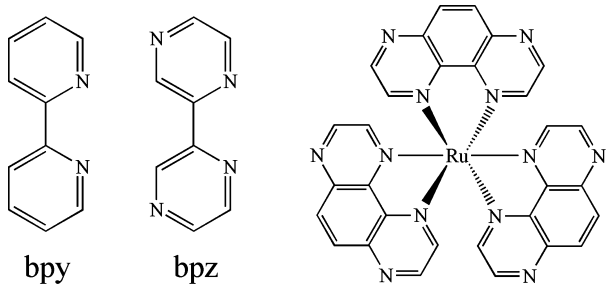

generally agreed that the emitting states are triplet metal-to-ligand charge-transfer states (MLCT), the controversy lies in the nature of the electronic structure of these states: in homoleptic complexes, the emitting state(s) can be described either with an electron localized on a single ligand or delocalized over all of them. The strength of the interligand coupling determines which situation can occur. Experimental evidence is available showing that, in solution, the excited electron is initially localized during the electronic transition[5] and that the relaxed excited-state is best described with one reduced ligand and two neutral ones.[6] However, the speed of the electron exchange between ligands is still debated. Malone et al.[7] indicate that it happens in a few tens of picoseconds, Yeh et al.[8] in a few picoseconds, whereas Wallin et al.[9] suggest that ultrafast interligand randomization of the excitation in the MLCT state is achieved in a few hundred femtoseconds. In the solid state, Yersin et al. clearly showed that the lowest excited states of $[Ru(bpy)_3]^{2+}$ cannot be regarded as being localized.[10] From a structural point of view, data are sparse. In 2006, Gawelda et al.[11] reported a Ru−N bond contraction of 0.037 ± 0.019 Å in the excited state of $[Ru(bpy)_3]^{2+}$, as compared to the ground state, using an X-ray absorption experiment in aqueous solution. This bond contraction is in good agreement with the value obtained by DFT calculations on the same complex.[12]

We have recently published a thorough comparison of the lowest triplet excited states of $[Ru(bpz)_3]^{2+}$ and the tris-bipyridine ruthenium(II) $[Ru(bpy)_3]^{2+}$ complexes.[12] The main conclusions of this study were that it is not sufficient to consider the MLCT states in the photoreactivity of these complexes: in fact, the triplet metal-centered (MC) state was shown to be of great importance. It has a rather unusual geometry, strongly displaced from the ground-state structure, which could lead to rapid dechelation or which could react readily with its environment. Experimentally, it is assumed that this state does not emit and leads either to fast radiationless deactivation or photoproducts with solvent molecules.[2] This kind of state is very often mentioned as playing an important role,[2] via internal conversion processes, in the lifetime of the MLCT states, but no direct observation of their relative energy position has ever been reported.

The $[Ru(tap)_3]^{2+}$ complex has been studied less than the $[Ru(bpz)_3]^{2+}$ and $[Ru(bpy)_3]^{2+}$ complexes. A crystallographic structure, which does not show the expected 3-fold symmetry axis, has been obtained by Piccinni-Leopardi et al.[13] The synthesis, spectroscopic, and electrochemical properties have been reported by Kirsch-De Mesmaeker et al.[14] and a density functional theory (DFT) study on the electronic structure and properties of the ground state has been undertaken by Zheng et al.[15] and by Atsumi et al.[16] Because of their photoreactivity with nucleic acids and amino acids, these kinds of ruthenium complexes are very interesting potent agents in photodynamic therapy.

In this work, we present a theoretical study of the ground and the lowest triplet excited states of the $[Ru(tap)_3]^{2+}$ complex. In particular, we have investigated the problem of the electron localization in the MLCT states for the first time and explored the MLCT-MC equilibration reaction path. The article is organized as follows: after some computational details, we present in section 3 the results and discussion in which a study of the ground-state is presented, followed by its Franck−Condon excited states as given by time-dependent DFT (TD-DFT). Then, we discuss the electronic structures of the MLCT and MC triplet states using DFT. Finally, the MLCT-MC equilibrium is investigated.

2. Computational Details

DFT and TD-DFT calculations were performed using the *NWCHEM*[17] and *Gaussian 03*[18] packages. The TD-DFT approach promises a way forward to study excited states of large metallic complexes[19] and to model their interaction with large biological systems.[20] The B3LYP functional was used throughout with a rather large basis set: a Stuttgart relativistic

(5) Oh, D. H.; Boxer, S. G. *J. Am. Chem. Soc.* **1989**, *111*, 1130–1131.
(6) (a) Bradley, P. G.; Kress, N.; Hornberger, B. A.; Dallinger, R. F.; Woodruff, W. H. *J. Am. Chem. Soc.* **1981**, *103*, 7441–7446. (b) Smothers, W. K.; Wrighton, M. S. *J. Am. Chem. Soc.* **1983**, *105*, 1067–1069. (c) Webb, M. A.; Knorr, F. J.; McHale, J. L. *J. Raman. Spectrosc.* **2001**, *32*, 481–485. (d) Saes, M.; Bressler, C.; Abela, R.; Grolimund, D.; Johnson, S. L.; Heimann, P. A.; Chergui, M. *Phys. Rev. Lett.* **2003**, *90*, 047403.
(7) Malone, R. A.; Kelley, D. F. *J. Chem. Phys.* **1991**, *95*, 8970–8976.
(8) Yeh, A. T.; Shank, C. V.; McCusker, J. K. *Science* **2000**, *289*, 935–938.
(9) Wallin, S.; Davidsson, J.; Modin, J.; Hammarström, L. *J. Phys. Chem. A* **2005**, *109*, 4697–4704.
(10) Yersin, H.; Braun, D. *Coord. Chem. Rev.* **1991**, *111*, 39–46.
(11) Gawelda, W.; Johnson, M.; de Groot, F. M. F.; Abela, R.; Bressler, C.; Chergui, M. *J. Am. Chem. Soc.* **2006**, *128*, 5001–5009.
(12) Alary, F.; Heully, J.-L.; Bijeire, L.; Vicendo, P. *Inorg. Chem.* **2007**, *46*, 3154–3165.
(13) Piccinni-Leopardi, C.; Van Meerssche, M.; Declercq, J. P.; Germain, G. *Bull. Soc. Chim. Belg.* **1987**, *96*, 79–80.
(14) Kirsch-De Mesmaeker, A.; Nasielski-Hinkens, R.; Maetens, D.; Pauwels, D.; Nasielski, J. *Inorg. Chem.* **1984**, *23*, 377–379.
(15) Zheng, K. C.; Wang, J. P.; Shen, Y.; Peng, W. L.; Yun, F. C. *J. Chem. Soc., Dalton Trans.* **2002**, *111*, 116.
(16) Atsumi, M.; González, L.; Daniel, C. *J. Photochem. Photobiol. A: Chem.* **2007**, *190*, 310–320.
(17) Bylaska, E. J.;. de Jong, W. A.;. Kowalski, K.;. Straatsma, T. P.;. Valiev, M.;. Wang, D.;. Aprà, E.;. Windus, T. L.;. Hirata, S.;. Hackler, M. T.;. Zhao, Y.;. Fan, P.-D.;. Harrison, R. J.;. Dupuis, M.;. Smith, D. M. A.;. Nieplocha, J.;. Tipparaju, V.;. Krishnan, M.;. Auer, A. A.;. Nooijen, M.;. Brown, E.;. Cisneros, G.;. Fann, G. I.;. Früchtl, H.;. Garza, J.;. Hirao, K.;. Kendall, R.;. Nichols, J. A.;. Tsemekhman, K.;. Wolinski, K.;. Anchell, J.;. Bernholdt, D.;. Borowski, P.;. Clark, T.;. Clerc, D.;. Dachsel, H.;. Deegan, M.;. Dyall, K.;. Elwood, D.;. Glendening, E.;. Gutowski, M.;. Hess, A.;. Jaffe, J.;. Johnson, B.;. Ju, J.;. Kobayashi, R.;. Kutteh, R.;. Lin, Z.;. Littlefield, R.;. Long, X.;. Meng, B.;. Nakajima, T.;. Niu, S.;. Pollack, L.;. Rosing, M.;. Sandrone, G.;. Stave, M.;. Taylor, H.;. Thomas, G.;. van Lenthe, J.;. Wong, A.;. Zhang, Z. *NWChem, A Computational Chemistry Package for Parallel Computers, Version 5.0*; Pacific Northwest National Laboratory: Richland, Washington, 2006.

small-core effective potential[21] for ruthenium with its basis augmented by an *f* polarization function with an exponent of 0.96, a triple-ζ plus polarization basis set (Ahlrichs pVTZ)[22] was used for the carbon and nitrogen atoms, and a double-ζ plus polarization basis set (Ahlrichs pVDZ)[22] was used for hydrogen atoms. Two kinds of calculations were performed:

(i) Δ-SCF calculations that yield the energy difference between the triplet excited states at their optimized geometries and the closed-shell ground-state at the same geometry. This is a simple and reliable way to obtain emission energies. All of the triplet states were computed using unrestricted wave functions, whereas a restricted wave function was used for the singlet ground state.

(ii) TD-DFT calculations, which are performed at the ground-state geometry and which give the vertical absorption energies and the transition dipole moments. The asymptotic correction of Hirata et al.[23] was used. The lowest 15 triplet and 15 singlet roots were computed.

In some cases TD-DFT shows some important failures in long-range charge-transfer excited states. Theoretically, this has been explained by Dreuw[24] and Hieringer,[25] who showed that, in case of failure, the whole TD-DFT calculation gives similar results to those obtained by taking the energy difference of the orbital energies of the electron-accepting and electron-donating molecular orbitals. This remains true even in the case of hybrid functionals such as B3LYP. In our case, we have checked that this was not the case. Indeed, there is a substantial difference between the excitation energies given by TD-DFT and those given by eigenvalue differences. Moreover, TD-DFT has been shown to describe the MLCT states of large ruthenium complexes correctly, by comparison of the computed absorption spectra with experimental ones and in some cases with accurate muti-configurational calculations (CASSCF/CASPT2).[16,26]

Table 1. Computational Results of the Main Bond Lengths (Angstroms) and Bond Angles (Degrees) for the Ground State (GS) and for the MLCT $^3A_2$ Excited State of $[Ru(tap)_3]^{2+}$ in D_3 Symmetry

	GS	MLCT $^3A_2$	expt[a]
Ru−N	2.104	2.098	2.065
>C−N	1.363	1.370	-
>C−C<	1.416	1.403	-
N_1−Ru−N_2	79.4	79.7	80.1
N_1−Ru−N_4	173.2	174.2	172.4

[a] Ref 13.

Because of the inherent symmetry of the different excited states of this complex, it is possible to compute different electronic states by a suitable choice of guess vectors. In this way, three triplet MLCT states, one of D_3 symmetry and two of C_2 symmetry and two triplet MC states, were obtained and characterized at the B3LYP level. Spin contamination was negligible, with $\langle S^{**}2\rangle$ values never exceeding 2.016. For each electronic state, geometry optimizations were first performed with the *NWCHEM* program without any symmetry constraints. All of the structures obtained display either D_3 or C_2 symmetry. These structures were used to start symmetry-constrained geometry optimizations with tight convergence criteria and an ultrafine integration grid using *Gaussian 03*. The stability of each unrestricted triplet wave function obtained was analyzed before computing the analytical harmonic vibrational frequencies. Only the wave function of the MLCT ^3A state was found to be unstable, meaning that a lower-energy wave function of the same spin multiplicity exists (Figure S1 in the Supporting Information). As a consequence, the coupled-perturbed Hartree−Fock (CPHF) method used in determining analytical frequencies is not physically meaningful. In this particular case, we performed the harmonic frequency calculation numerically using small Cartesian displacements.

DFT energies were also recomputed using the conductor-like polarizable continuum model (CPCM)[18] with solvent acetonitrile at the different optimized structures in vacuum. The spin−orbit interactions between the singlet and triplet states have not been taken into account in this study.

3. Results and Discussion

3.1. Ground State. The principal geometrical parameters of this complex are reported in Table 1 and the molecular structure is shown in Figure 1. The symmetry of the true minima is D_3. The Ru−N coordination distance of 2.104 Å agrees with the value obtained by Atsumi et al.[16] It is also very similar to the coordination distances calculated in the $[Ru(bpy)_3]^{2+}$ and $[Ru(bpz)_3]^{2+}$ complexes.[12] Experimentally $[Ru(tap)_3]^{2+}$ is not found to be rigorously of D_3 symmetry, but the average Ru−N distance is 2.065 Å, the average angle

(18) Frisch, M. J.;. Trucks, G. W.;. Schlegel, H. B.;. Scuseria, G. E.;. Robb, M. A.;. Cheeseman, J. R.;. Montgomery, J. A.;. Vreven, T.;. Kudin, K. N.;. Burant, J. C.;. Millam, J. M.;. Iyengar, S. S.; Tomasi, J.;. Barone, V.;. Mennucci, B.;. Cossi, M.;. Scalmani, G.;. Rega, N.;. Petersson, G. A.;. Nakatsuji, H.;. Hada, M.;. Ehara, M.;. Toyota, K.;. Fukuda, R.;. Hasegawa, J.;. Ishida, M.;. Nakajima, T.;. Honda, Y.;. Kitao, O.;. Nakai, H.;. Klene, M.;. Li, X.;. Knox, J. E.;. Hratchian, H. P.;. Cross, J. B.;. Bakken, V.;. Adamo, C.;. Jaramillo, J.;. Gomperts, R.;. Stratmann, R. E.;. Yazyev, O.;. Austin, A. J.;. Cammi, R.;. Pomelli, C.;. Ochterski, J. W.;. Ayala, P. Y.;. Morokuma, K.;. Voth, G. A.;. Salvador, P.;. Dannenberg, J. J.;. Zakrzewski, V. G.; Dapprich, S.;. Daniels, A. D.;. Strain, M. C.;. Farkas, O.;. Malick, D. K.;. Rabuck, A. D.;. Raghavachari, K.;. Foresman, J. B.;. Ortiz, J. V.;. Cui, Q.;. Baboul, A. G.;. Clifford, S.;. Cioslowski, J.;. Stefanov, B. B.;. Liu, G.;. Liashenko, A.;. Piskorz, P.;. Komaromi, I.;. Martin, R. L.;. Fox, D. J.;. Keith, T.;. Al-Laham, M. A.;. Peng, C. Y.; Nanayakkara, A.;. Challacombe, M.;. Gill, P. M. W.;. Johnson, B.;. Chen, W.;. Wong, M. W.;. Gonzalez, C.;. Pople. J. A. *Gaussian 03,* Revision D.01; Gaussian, Inc.: Wallingford, CT, 2004.
(19) Guillemoles, J.-F.; Barone, V.; Joubert, L.; Adamo, C. *J. Chem. Phys. A* **2002**, *106*, 11354–11360.
(20) Morgado, C.; Vincent, M. A.; Hillier, I. H.; Shan, X. *Phys. Chem. Chem. Phys.* **2007**, *9*, 448–451.
(21) Dolg, M.; Stoll, H.; Preuss, H.; Pitzer, R. M. *J. Phys. Chem.* **1993**, *97*, 5852–5859.
(22) Schäfer, A.; Horn, H.; Ahlrichs, R. *J. Chem. Phys.* **1992**, *97*, 2571–2577.
(23) Hirata, S.; Zhan, C.-G.; Aprà, E.; Windus, T. L.; Dixon, D. A. *J. Phys. Chem. A* **2003**, *107*, 10154–10158.
(24) Dreuw, A.; Weisman, J. L.; Head-Gordon, M. *J. Chem. Phys.* **2003**, *119*, 2943–2946.
(25) Hieringer, W.; Görling, A. *Chem. Phys. Lett.* **2006**, *419*, 557–562.
(26) (a) Turki, M.; Daniel, C.; Zális, S.; Vlcek, A., Jr.; van Slageren, J.; Stufkens; D. J., *J. Am. Chem. Soc.* **2001**, *123*, 11431–11440. (b) Zális, S.; Ben Amor, N.; Daniel, C. *Inorg. Chem.* **2004**, *43*, 7978–7985. (c) Ben Amor, N.; Zális, S.; Daniel, C. *Int. J. Quantum Chem.* **2006**, *106*, 2458–2469. (d) Vlcek, A.; Zális, S. *Coord. Chem. Rev.* **2007**, *251*, 258–287.

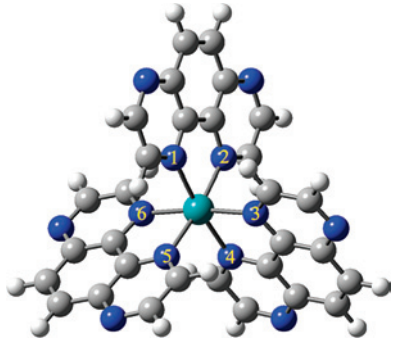

Figure 1. Structure of the $[Ru(tap)_3]^{2+}$ singlet ground-state and numbering of the atoms.

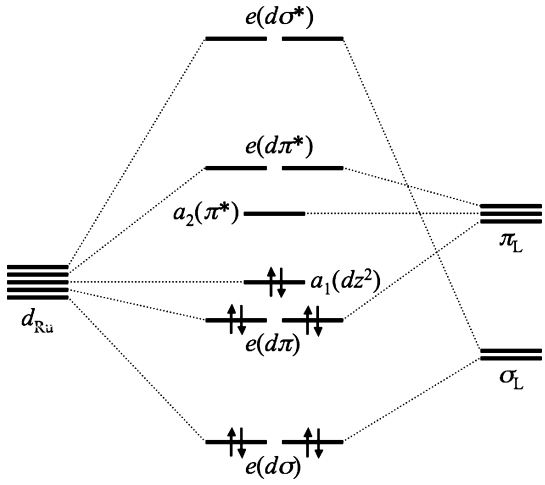

Figure 2. Simplified molecular orbital correlation diagram of $[Ru(tap)_3]^{2+}$ in D_3 symmetry.

N_1-Ru-N_2 is 80.1°, and the average angle N_1-Ru-N_4 is 172.4°.[13] The largest difference with experiment is thus observed for the coordination distance that is slightly overestimated (ca. 0.04 Å), as usually observed with hybrid functional calculations.[27]

A simplified molecular orbital correlation diagram representing the ground-state electronic configuration in D_3 symmetry is shown in Figure 2. The highest occupied orbitals are two degenerate orbitals of e symmetry (noted dπ with dominant d character of the metal) and above these the HOMO of a_1 symmetry corresponding to the pure metal orbital dz^2. The first empty orbital is a pure ligand orbital of a_2 symmetry (LUMO), and above this, we find two degenerate e orbitals with a small contribution from the metal (dπ*). Far above these three empty orbitals lie the two empty antibonding dσ* orbitals, corresponding to the e_g orbitals in the O_h point group.[28]

3.2. Excited States. 3.2.1. Excitation Energies. The absorption spectrum recorded by Masschelein et al.[29] in the solvent acetonitrile shows two maxima at 437 nm (2.84 eV) and 408 nm (3.04 eV) with similar amplitudes and one more intense peak at 276 nm (4.49 eV). Our calculations with the TD-DFT method, presented in Table 2, show a rather good agreement with these experimental observations. Table 2 only shows vertical transitions with a significant oscillator strength in the investigated energetic region, all of them leading to MLCT states. The largest and observed ones lead to states of E symmetry (polarization perpendicular to the C_3 axis), which is expected because the C_3 axis does not point toward any particular part of the molecule. This is also the reason why the first absorbing transitions are not HOMO−LUMO. The positions of the triplet states (at the geometry of the ground state) are also given in Table 2. Three triplet states are predicted in a very narrow interval of 0.06 eV, all of them being of MLCT nature. When presenting the ground-state results, we mentioned that the dσ* orbitals are found at very high energy. This is confirmed by the fact that none of the first 15 transitions involves these orbitals (i.e., MC states).

Table 2. Computed TD-DFT Vertical Excitation Energies ΔE (eV) with Significant Oscillator Strengths f

singlet (expt values = 2.84, 3.04 eV)			triplet	
ΔE	Configurations[a]	f	ΔE	Configurations
2.847	$e(d\pi_1) \rightarrow a_2(\pi^*)$	0.008	2.437	$a_1(dz^2) \rightarrow e(d\pi_1^*)$
2.847	$e(d\pi_2) \rightarrow a_2(\pi^*)$	0.008	2.437	$a_1(dz^2) \rightarrow e(d\pi_2^*)$
2.985	$e(d\pi_1) \rightarrow e(d\pi_2^*)$ $e(d\pi_2) \rightarrow e(d\pi_1^*)$	0.053	2.481	$a_1(dz^2) \rightarrow a_2(\pi^*)$
2.985	$e(d\pi_1) \rightarrow e(d\pi_1^*)$ $e(d\pi_2) \rightarrow e(d\pi_2^*)$	0.053	2.489	$e(d\pi_1) \rightarrow e(d\pi_2^*)$ $e(d\pi_2) \rightarrow e(d\pi_1^*)$
3.142	$a_1(dz^2) \rightarrow e(d\pi_i^*)$	0.058	2.609	$e(d\pi_1) \rightarrow e(d\pi_2^*)$ $e(d\pi_2) \rightarrow e(d\pi_1^*)$ $e(d\pi_2) \rightarrow a_2(\pi^*)$
3.142	$a_1(dz^2) \rightarrow e(d\pi_i^*)$	0.058	2.609	$e(d\pi_1) \rightarrow e(d\pi_1^*)$ $e(d\pi_2) \rightarrow e(d\pi_2^*)$ $e(d\pi_1) \rightarrow a_2(\pi^*)$
3.254	$e(d\pi_1) \rightarrow e(\pi_i^*)$ $e(d\pi_2) \rightarrow e(\pi_i^*)$	0.111	2.696	$e(d\pi_1) \rightarrow a_2(\pi^*)$
3.254	$e(d\pi_1) \rightarrow e(\pi_i^*)$ $e(d\pi_2) \rightarrow e(\pi_i^*)$	0.111	2.696	$e(d\pi_2) \rightarrow a_2(\pi^*)$

[a] i refers to higher virtual orbitals not shown in Figure 2.

3.2.2. Triplet MLCT States. By performing preliminary geometry optimizations in the C_1 point group with different starting guess vectors, two minima were located on MLCT triplet state potential energy surfaces. These structures were also found in the complexes with bpy and bpz ligands.[12]

The first minimum conserves D_3 symmetry and has almost the same geometry as the ground state. Its main geometrical parameters are given in Table 1 for comparison. The computed contraction of the Ru−N bond (<0.01 Å) in this D_3 MLCT state is less pronounced than those computed in the case of $[Ru(bpy)_3]^{2+}$ and $[Ru(bpz)_3]^{2+}$ complexes. This weaker contraction may be due to stronger steric constraints of the more rigid tap ligand. The electronic configuration is $a_1(dz^2)^1a_2(\pi^*)^1$, and the corresponding singly occupied orbitals are shown in Figure 3. This electronic state will be denoted MLCT $^3A_2$. The ruthenium is now in the oxidation state +III, and one electron is equally distributed over the three ligands in the $a_2(\pi^*)$ orbital. The emission calculated by Δ-SCF is 2.31 eV, in fairly good agreement with the available experimental data of 2.14 eV and within the typical accuracy expected from this method.

The second minimum has its symmetry reduced to C_2 because of Jahn−Teller distortion.[30] Because the electronic

(27) Stoyanov, S. R.; Villegas, J. M.; Rillema, D. P. *Inorg. Chem.* **2002**, *41*, 2941–2945.
(28) Jean, Y. *In Molecular Orbitals of Transition Metal Complexes*; Oxford University Press: New York, 2005.
(29) Masschelein, A.; Jacquet, L.; Kirsch-De Mesmaeker, A.; Nasielski, J. *Inorg. Chem.* **1990**, *29*, 855–860.

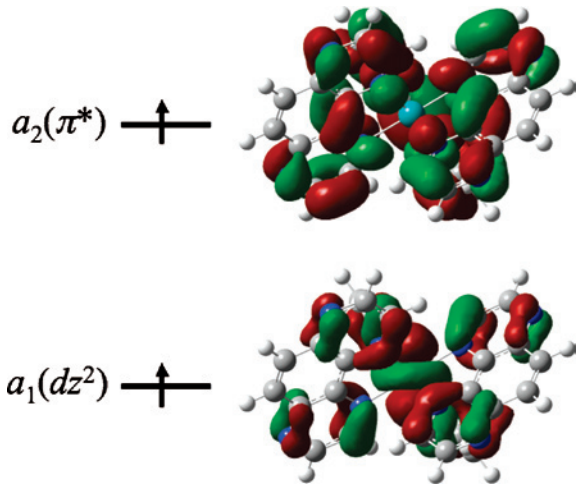

Figure 3. Electronic configuration and singly occupied molecular orbitals of the MLCT $^3A_2$ state.

state associated with this C_2 minimum correlates with a doubly degenerate MLCT ^3E state ($a_1(dz^2)^1e(d\pi^*)^1$) in D_3 symmetry, as shown in Figure 4, it is expected to undergo such a distortion. Two different electronic states arise from the doubly degenerate ^3E state upon Jahn−Teller distortion (Figure 4). One corresponds to the configuration $a(dz^2)^1b(d\pi^*)^1$ and will be denoted MLCT ^3B, whereas the electronic configuration of the other state, denoted MLCT ^3A, is $a(dz^2)^1a(d\pi^*)^1$, with both $b(d\pi^*)$ and $a(d\pi^*)$ correlating with the doubly degenerate $e(d\pi^*)$ orbitals. We found that the MLCT ^3B state is a true minimum, whereas the MLCT ^3A state is a transition state connecting two equivalent minima of the MLCT ^3B potential energy surface (Figure S1 in the Supporting Information). This is the usual topology in Jahn−Teller systems with a 3-fold symmetry axis (e.g., $E\otimes e$ Jahn−Teller problem):[31] a conical intersection (Jahn−Teller crossing) enforced by symmetry corresponding to the ^3E state is predicted to induce symmetry breaking along a C_2 distortion coordinate, leading to three equivalent minima (MLCT ^3B) and three equivalent transition states (MLCT ^3A) lying at the bottom of a moat encircling the conical intersection (Figure 5).

The main geometrical parameters for the MLCT ^3B minimum and MLCT ^3A transition state are given in Table 3. An important point worth noting is the fact that the distortion from D_3 symmetry is rather weak, indicating a weak linear (first-order) coupling.[31] At the MLCT ^3B minimum geometry, the ligand bearing the C_2 axis has two Ru−N bond lengths of 2.120 Å, whereas the two other ligands have slightly different coordination distances, each ligand having one Ru−N distance of 2.098 Å and one of 2.089 Å. It is also notable that the MLCT ^3A transition state structure displays very similar coordination distances. This is not surprising because the nature of the singly occupied orbitals is very similar in the two states. The main difference lies in the symmetry of the $b(d\pi^*)$ and $a(d\pi^*)$ orbitals. One

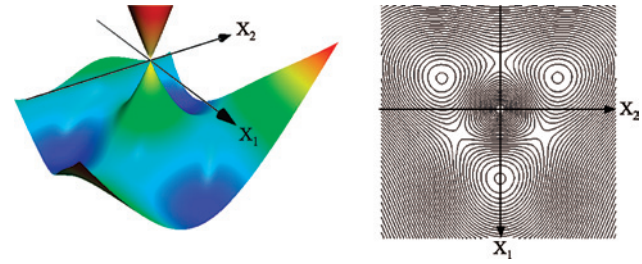

Figure 5. Schematic representation of a moat around a Jahn−Teller D_3 crossing showing the three symmetry-equivalent minima and transition states: 3D representation (the tricorn, left) and equipotential contour plot (right) in the space of the two degeneracy-lifting coordinates X_1 and X_2 (i.e., along the gradient difference and derivative coupling vectors). Arbitrary colors have been used.

Table 3. Computational Results of the Main Bond Lengths (Angstroms) and Bond Angles (Degrees) for the MLCT ^3B and MLCT ^3A states of $[Ru(tap)_3]^{2+}$ in C_2 Symmetry

	MLCT ^3B	MLCT ^3A
$Ru-N_1$	2.120	2.119
$Ru-N_2$	2.120	2.119
$Ru-N_3$	2.098	2.104
$Ru-N_4$	2.089	2.086
$Ru-N_5$	2.089	2.086
$Ru-N_6$	2.098	2.104
$>C_1-C_2<^a$	1.409	1.415
$>C_3-C_4<^b$	1.402	1.399
$>C_5-C_6<^c$	1.402	1.399
N_1-Ru-N_2	79.1	79.2
N_3-Ru-N_6	175.1	174.1
N_4-Ru-N_5	88.9	86.0

[a] Bond length between carbon atoms bonded to N_1 and N_2. [b] Bond length between carbon atoms bonded to N_3 and N_4. [c] Bond length between carbon atoms bonded to N_5 and N_6.

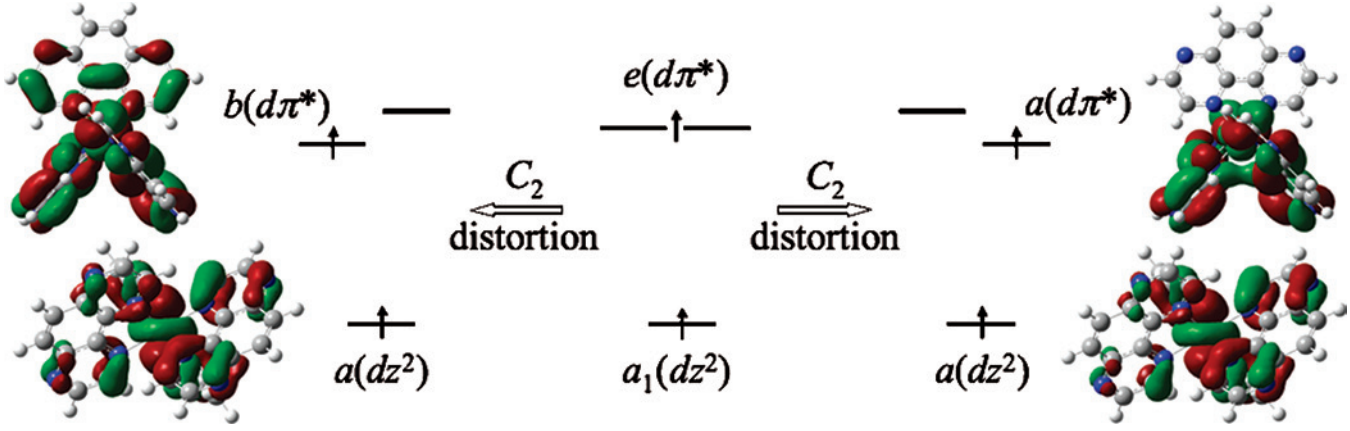

Figure 4. Electronic configurations and singly occupied molecular orbitals of the MLCT ^3B (left) and MLCT ^3A (right) states, following Jahn−Teller C_2 distortion of the doubly degenerate MLCT ^3E state (center).

Table 4. Computational Results of the Main Bond Lengths (Angstroms) and Bond Angles (Degrees) for the MC ^3A and MC ^3B States of $[Ru(tap)_3]^{2+}$ in C_2 Symmetry

	MC ^3A	MC ^3B
$Ru-N_1$	2.120	2.359
$Ru-N_2$	2.120	2.359
$Ru-N_3$	2.516	2.096
$Ru-N_4$	2.142	2.276
$Ru-N_5$	2.142	2.276
$Ru-N_6$	2.516	2.096
$>C_1-C_2<$[a]	1.413	1.432
$>C_3-C_4<$[b]	1.432	1.422
$>C_5-C_6<$[c]	1.432	1.422
N_1-Ru-N_2	78.8	71.6
N_3-Ru-N_6	167.6	174.5
N_4-Ru-N_5	87.8	95.0

[a] Bond length between carbon atoms bonded to N_1 and N_2. [b] Bond length between carbon atoms bonded to N_3 and N_4. [c] Bond length between carbon atoms bonded to N_5 and N_6.

can see that the $b(d\pi^*)$ orbital has some bonding character in a few C−C and C−N bonds on the ligand bearing the C_2 axis, whereas no electron density is present on this ligand in the $a(d\pi^*)$ orbital for symmetry reasons (Figure 4). This is illustrated by the shorter C_1-C_2 bond for the B state in Table 3. Also, there is an interligand π-bonding interaction in $a(d\pi^*)$, which does not exist in $b(d\pi^*)$. As a result, the N_4-Ru-N_5 angle is smaller in the ^3A state. The Δ-SCF emission energy is 2.28 eV, very similar to the one obtained for the MLCT $^3A_2$ state.

We can now address the controversial problem of the localization or delocalization of the excitation, that is, we are concerned with the description of the MLCT state of $[Ru(tap)_3]^{2+}$ as $[Ru^{3+}(tap)_2(tap^-)]^{2+}$ or as $[Ru^{3+}(tap^{-1/3})_3]^{2+}$. The former case corresponds to a situation in which the promoted electron resides for a measurable amount of time on a single ligand, whereas the latter case describes a situation in which the electron is completely shared by the three ligands or it undergoes hopping from ligand to ligand faster than the resolution time of the monitoring technique.[2] Our results are unambiguous as far as the MLCT states investigated in this work are concerned. The MLCT ^3B state, which is the lowest triplet MLCT state found, displays a weak C_2 distortion, and the singly occupied orbital $b(d\pi^*)$ displays a large electron density on the three ligands. Moreover, the pseudo-rotation barrier[31] around the moat of the lowest adiabatic triplet potential energy surface (energy difference between the ^3B minimum and the ^3A transition state) is only 0.5 kcal/mol. In acetonitrile solvent using CPCM, the barrier is reduced to 0.2 kcal/mol due to the larger dipole moment of ^3A. Thus, in this electronic state, all the extrema points (minima and transition states) have approximately the same energy. This means that the quadratic (second-order) coupling is very weak to negligible (at least in this approximation of the calculations). Thus, there is a trough along which the system performs free pseudo-rotation, leading to a time-averaged D_3 structure. Moreover, the MLCT $^3A_2$ state, which lies less than 0.1 and 0.6 kcal/mol above MLCT ^3B in vacuum and in acetonitrile, respectively, is a real D_3 minimum, where the promoted electron is equally shared between the three ligands. Thus, on the basis of these results, it appears that the two lowest MLCT triplet states should be viewed as $[Ru^{3+}(tap^{-1/3})_3]^{2+}$. This is consistent with the ultrafast electron hopping from one ligand to another, observed by a femtosecond transient absorption anisotropy study.[9]

3.2.3. Triplet MC States. Starting with a suitable guess vector (i.e., a hole in the $a(dz^2)$ orbital and one electron in the $a(d\sigma^*)$ orbital), geometry optimization leads to an unusual structure of C_2 symmetry (Figure S2 in Supporting Information). Its principal geometrical parameters are given in Table 4. One can see that two ligands now have a Ru−N bond length of 2.516 Å and another one of 2.142 Å, whereas the third ligand, bearing the C_2 axis, has two coordination distances of 2.120 Å. Thus, two ligands are monocoordinated, whereas the third one remains bicoordinated, resulting in two monodentate and one bidentate tap ligands. This electronic state with the configuration $a(dz^2)^1a(d\sigma^*)^1$ is denoted MC ^3A, and the antibonding $a(d\sigma^*)$ orbital responsible for the decoordination is shown in Figure 6. This structure is a true minimum on the MC triplet potential energy surface, and it may readily react with its environment via the two vacant coordination sites on the metal. In fact, this state correlates with the doubly degenerate MC ^3E state $(a_1(dz^2)^1e(d\sigma^*)^1)$ in D_3 symmetry, as shown in Figure 6, and its C_2 structure results from Jahn−Teller distortion. As for the MLCT states described above, another state with the configuration

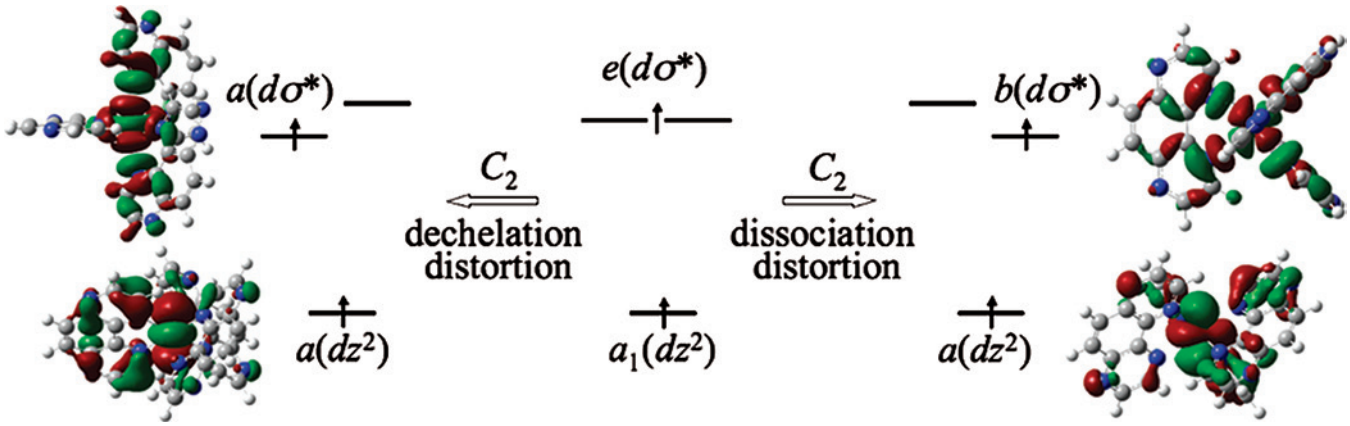

Figure 6. Electronic configurations and singly occupied molecular orbitals of the MC ^3A (left) and MLCT ^3B (right) states, following Jahn−Teller C_2 distortion of the doubly degenerate MC ^3E state (center).

Table 5. Thermochemical Quantities for $[Ru(tap)_3]^{2+}$ and $[Ru(bpy)_3]^{2+}$ in kcal/mol and Relative to the MC ^3A State

	$[Ru(tap)_3]^{2+}$			$[Ru(bpy)_3]^{2+}$		
	MLCT $^3A_2$	MLCT ^3B	MC ^3A	MLCT $^3A_2$	MLCT ^3B	MC ^3A
ΔE	6.98	6.93	0	1.96	1.78	0
$\Delta(E + \text{ZPE})$	5.00	5.18	0	0.49	0.55	0
$\Delta(E + \text{CPCM})$ [a]	4.61	4.05	0	0.19	−0.61	0
At 298.15 K						
ΔH	4.72	4.84	0	0.05	0.05	0
ΔG	7.04	6.76	0	3.15	2.75	0
ΔG_{solv} [b]	4.67	3.89	0	1.38	0.36	0
At 77 K						
ΔH	4.85	5.02	0	0.28	0.33	0
ΔG	5.17	5.38	0	0.92	0.84	0
ΔG_{solv} [b]	2.80	2.51	0	−0.85	−1.55	0

[a] Calculation using the conductor-like polarizable continuum model with solvent acetonitrile. [b] Estimation of ΔG in acetonitrile using the gas phase partition functions. Structures and vibrational levels have not been recomputed with CPCM (Computational Details).

$a(dz^2)^1 b(d\sigma^*)^1$ and denoted MC ^3B correlates with MC ^3E, as shown in Figure 6. At its optimized structure, one ligand has its two coordination distances stretched to 2.359 Å, whereas the other two ligands share a long Ru−N bond (2.276 Å) and a shorter one (2.096 Å). Thus, one ligand is predissociated at this geometry. This can be explained by the nature of the $b(d\sigma^*)$ orbital, which is antibonding along four Ru−N bonds, two of which belong to the same tap ligand. Thus, one ligand can easily predissociate, whereas the other two tap ligands have some monodentate character. This structure was found to be a transition state connecting two symmetry-equivalent minima of the MC ^3A potential energy surface (Figure S3 in the Supporting Information). The potential energy surface topology is again similar to the one shown in Figure 5. The main difference with the MLCT ^3B and ^3A states is that both linear and quadratic couplings are stronger in these MC states. Indeed, the distortion from D_3 symmetry is much more pronounced, and the pseudo-rotation barrier between the three equivalent MC ^3A minima is larger (3.0 and 2.7 kcal/mol in vacuum and in acetonitrile, respectively).

The emission energy (if this state could irradiate) calculated by Δ-SCF is 0.96 eV; a region of the spectrum that is seldom scrutinized. It should also be noted that if one optimizes the geometry of the ground state starting from the MC ^3A geometry, the molecule does not dissociate but returns to the ground-state D_3 geometry.

3.2.4. MLCT-MC Equilibrium. Using the data obtained from calculating the harmonic frequencies, we can obtain the zero-point energy (ZPE) and thermochemical quantities such as the enthalpy H, the entropy S, and the Gibbs free energy G. These quantities have been calculated for both $[Ru(tap)_3]^{2+}$ and $[Ru(bpy)_3]^{2+}$ at 298.15 and 77 K. Table 5 collects all of the results in terms of relative energies.

First, one can observe that the MC ^3A state is the lowest excited state in both systems at room temperature and in vacuum. When taking interactions with the acetonitrile solvent into account, the MLCT states are stabilized more than the MC state because of the charge-transfer nature of the MLCT states, reducing the energy difference ΔE. Second, one can see that the main difference between the two complexes is that the MC ^3A state has a similar energy compared to the MLCT states in $[Ru(bpy)_3]^{2+}$, whereas it is appreciably lower in $[Ru(tap)_3]^{2+}$. This result is in agreement with the experimental observations of larger dechelation (via the MC state) and smaller emission (via the MLCT states) quantum yields of $[Ru(tap)_3]^{2+}$ compared to those of $[Ru(bpy)_3]^{2+}$ in acetonitrile.[29]

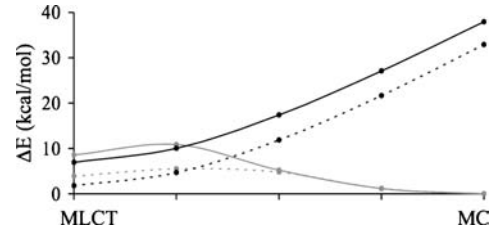

Figure 7. Potential energy profiles along an approximate MLCT → MC reaction path. ^3B energy profile is in black, ^3A energy profile is in gray. Results for $[Ru(tap)_3]^{2+}$ in full line, results for $[Ru(bpy)_3]^{2+}$ in dashed line.

To obtain a better understanding of the MLCT → MC reaction path, we computed the energies of the ^3B and ^3A states at linearly interpolated geometries between the MLCT ^3B and the MC ^3A minima. The results are shown in Figure 7.

The black curves correspond to the MLCT ^3B energies. As the complex relaxes toward the MC minimum, the energy of this state increases as expected. The gray curves correspond to the ^3A energies. Starting from the MC geometry and moving toward the MLCT structure, the energy of the MC ^3A state increases as expected. Then, there is a change in the electronic nature of the adiabatic ^3A potential energy surface, which becomes the MLCT ^3A state. This means that there is an avoided crossing between the MLCT ^3A and MC ^3A states, giving rise to the barrier on the lowest ^3A adiabatic potential energy profile (Figure 7). However, as we know from subsection 3.2.2., the lowest MLCT state is ^3B, and this state crosses the MC ^3A state as shown in Figure 7. There is therefore a conical intersection between these two states encountered along the MLCT → MC reaction path. This means that the transition state connecting the MLCT ^3B and MC ^3A minima on the lowest triplet adiabatic potential energy surface must lie on the side of this crossing at a lower energy (Figure S4 in Supporting Information). Attempts to optimize this transition structure failed. However, although we cannot optimize the $^3B/^3A$ conical intersection at the level of calculation used in this study, the position of the $^3B/^3A$ crossing point in Figure 7 gives an upper-bound estimate for the barrier between the MLCT ^3B and MC ^3A minima in vacuum. Thus, the MLCT → MC barrier is estimated not to exceed 3 kcal/mol for both $[Ru(tap)_3]^{2+}$ and $[Ru(bpy)_3]^{2+}$. On the other hand, the MC → MLCT barrier is below 10 and 5 kcal/mol in $[Ru(tap)_3]^{2+}$ and $[Ru(bpy)_3]^{2+}$, respectively. We therefore expect the equilibrium to be more displaced toward the MC state in $[Ru(tap)_3]^{2+}$ compared to $[Ru(bpy)_3]^{2+}$ in vacuum, and, from a kinetic point of view, a faster return to the MLCT state can be predicted in $[Ru(bpy)_3]^{2+}$.

(30) Jahn, H. A.; Teller, E. *Proc. R. Soc. London, Ser. A* **1937**, *161*, 220.
(31) (a) Bersuker, I. B. *Chem. Rev.* **2001**, *101*, 1067–1114. (b) Bersuker, I. B. *In The Jahn-Teller Effect;* Cambridge: U. K., 2006.

Table 5 shows that these results are still qualitatively valid in acetonitrile. Note, however, that at a lower temperature, the MLCT states may become lower than the MC state in $[Ru(bpy)_3]^{2+}$. This result may look at variance with the experimental observations of a stronger emission in $[Ru(tap)_3]^{2+}$ at 77 K,[29] but the reason invoked for this behavior is based on the more efficient nonradiative decay from the MLCT states in $[Ru(bpy)_3]^{2+}$, a process that we have not studied in this work.

4. Conclusion

The theoretical study presented here has focused on the ground and lowest triplet excited states of the $[Ru(tap)_3]^{2+}$ complex. Both the TD-DFT absorption energies and Δ-SCF emission energies agree well with the experimental values. As in our previous study of the $[Ru(bpy)_3]^{2+}$ and $[Ru(bpz)_3]^{2+}$ complexes, our calculations revealed the presence of three low-lying minima corresponding to the MLCT $^3A_2$, the MLCT ^3B, and the MC ^3A states. The MLCT states are so close in energy that it is impossible to decide which is the lowest one. The MC state was found to be about 7 kcal/mol lower in vacuum.

We have characterized for the first time the extrema around the D_3 conical intersection due to Jahn−Teller effects. The MLCT ^3B state is a true minimum at its C_2 equilibrium geometry, whereas the MLCT ^3A state is a transition state connecting the ^3B minima. This transition state lies only 0.5 kcal/mol above the minima, resulting in a very small pseudorotational barrier around the moat. The structure of MLCT ^3B, while instantaneously slightly localized in C_2 symmetry, will dynamically have a time-averaged delocalized D_3 structure. Moreover, the MLCT $^3A_2$ state has a true D_3 minimum, meaning that no electron localization is expected in this electronic state. Therefore, in both studied triplet MLCT states, the promoted electron is delocalized on the three tap ligands, reinforcing the formal view of the complex in the lowest MLCT states as $[Ru^{3+}(tap^{-1/3})_3]^{2+}$.

Although the transition state between the MLCT and MC triplet states has not yet been characterized, determination of an approximate reaction path of the MLCT → MC conversion in $[Ru(tap)_3]^{2+}$ and $[Ru(bpy)_3]^{2+}$ reveals that the MC state is easily accessible from the MLCT state for both complexes. Examination of the backward conversion, that is MC → MLCT, indicates that populating the MLCT state will be more efficient in the $[Ru(bpy)_3]^{2+}$ complex. This finding can explain the higher photoinstability of $[Ru(tap)_3]^{2+}$ with respect to $[Ru(bpy)_3]^{2+}$.

Future work will aim at taking account of the spin−orbit interactions in the description of the electronic states involved in the emission spectrum. The present study has shed some light on the nature of the electronic states possibly involved in the photophysics and photochemistry of ruthenium polypyridyl complexes. The next aim will be to get some understanding of the photoreactivity of these complexes with biomolecules (e.g., DNA bases, amino acids, and proteins).

Acknowledgment. We thank CALMIP for access to computing resources.

Supporting Information Available: List of Cartesian coordinates of optimized DFT structures. Figure S1 for the transition vector of MLCT ^3A. Figure S2 for the structure of the MC ^3A minimum. Figure S3 for the transition vector of MC ^3B. Figure S4 for the illustration of a transition state on the side of a peaked conical intersection. This material is available free of charge via the Internet at http://pubs.acs.org.

IC800246T